Fine-scale structure of the extratropical tropopause region

T. Birner[1,2]

Received 1 June 2005; revised 3 November 2005; accepted 17 November 2005; published 25 February 2006.

[1] A vertically high resolved climatology of the thermal and wind structure of the extratropical tropopause region is presented. The climatology is based on data from 80 U.S. radiosonde stations covering the period 1998–2002. Time averages for each radiosonde station are computed using the tropopause as a common reference level for all vertical profiles within the mean. A strong inversion at the tropopause in the mean vertical temperature gradient is uncovered; that is, temperature strongly increases with altitude within the lowermost stratosphere. This tropopause inversion layer exists on average throughout the investigated extratropics (about 30°N to 70°N). Accordingly, the static stability parameter shows considerably enhanced values within the lowermost extratropical stratosphere compared to typical extratropical stratospheric values further aloft. Conventional averages are not able to capture the tropopause inversion layer. Mean profiles of the horizontal wind show behavior qualitatively corresponding to thermal wind balance. Winter and summer exhibit distinctly different climate states in the extratropical tropopause region. An approximated potential vorticity is considered and found to be close to well mixed within the troposphere as well as within the tropopause inversion layer. This suggests the view of the tropopause inversion layer as representing a dynamically active atmospheric layer. Some potential implications are discussed.

Citation: Birner, T. (2006), Fine-scale structure of the extratropical tropopause region, *J. Geophys. Res.*, *111*, D04104, doi:10.1029/2005JD006301.

1. Introduction

[2] There has been an increased recent interest in the global tropopause region (frequently called UTLS: Upper Troposphere and Lower Stratosphere). The tropopause region is distinct in many aspects: radiation, dynamics on a vast variety of scales, chemistry, and microphysics can play an equally important role. This strong connectivity amongst processes of different nature makes the tropopause region highly sensitive to climate change [e.g., *Shepherd*, 2002]. In fact, it has been proposed that features such as the tropopause height serve as a useful indicator of climate change [e.g., *Santer et al.*, 2003]. There has been also increased interest in stratosphere-to-troposphere coupling in recent years [e.g., *Baldwin and Dunkerton*, 1999] with some emphasis on stratospheric processes affecting tropospheric weather and climate [e.g., *Thompson and Wallace*, 1998; *Charlton et al.*, 2004]. Coupling between the stratosphere and the troposphere by definition involves the tropopause.

[3] Unfortunately, there is no unique concept of what constitutes the tropopause. Conventionally, troposphere and stratosphere are distinguished by means of their thermal stratification, measured by the temperature lapse rate $\gamma \equiv -\partial_z T$, where T is temperature and z is altitude. In the troposphere large-scale and small-scale turbulent motion lead to small (but stable) stratification (typically $\gamma \gtrsim 5$ K km^{-1}; that is, $N^2 \sim 1 \cdot 10^{-4}$ s^{-2}, where $N^2 = g\Theta^{-1}\partial_z\Theta$ is the buoyancy frequency, with g, acceleration due to gravity, and Θ, potential temperature), whereas the stratosphere is comparatively strongly stably stratified (typically $\gamma \lesssim 0$, i.e., $N^2 \gtrsim 4 \cdot 10^{-4}$ s^{-2}). The thermal tropopause is located at the lowest level at which γ falls below $\gamma_{TP} = 2$ K km^{-1}, if the average of γ between this level and all higher levels within 2 km remains below γ_{TP} [*World Meteorological Organization* (*WMO*), 1957]. Vertical temperature profiles are routinely measured by the radiosonde network. The thermal definition thus provides a very convenient way to determine the tropopause and is most widely used.

[4] The dynamical tropopause utilizes that Ertel's potential vorticity (PV, P) is conserved for adiabatic, frictionless motions by assigning the tropopause to the lowest level at which the PV exceeds a certain threshold P_{TP} [*WMO*, 1986]. Values of P_{TP} ranging between 1 and 4 PVU (1 PVU = 10^{-6} K m^2 kg^{-1} s^{-1}) can be found in the literature [e.g., *Reed*, 1955; *Shapiro*, 1980; *Hoerling et al.*, 1991; *Hoinka*, 1998].

[5] To further add to the confusion, there are also chemical tropopause definitions based on specific thresholds in the concentration of trace gases such as ozone [*Bethan et al.*, 1996]. A recent comparison of different tropopause definitions [*Pan et al.*, 2004] has revealed good agreement

[1]Deutsches Zentrum für Luft- und Raumfahrt, Institut für Physik der Atmosphäre, Oberpfaffenhofen, Wesseling, Germany.
[2]Now at Department of Physics, University of Toronto, Toronto, Ontario, Canada.

0148-0227/06/2005JD006301

between chemical and thermal tropopause definitions. However, in individual midlatitude upper tropospheric flow disturbances it is rather the material surface concept of the dynamical tropopause that shows good agreement with the chemically defined tropopause [*Bethan et al.*, 1996; *Wirth*, 2000].

[6] The extratropical tropopause is predominantly controlled by the large-scale turbulent mixing due to baroclinic eddies [e.g., *Schneider*, 2004]. This large-scale mixing tends to eliminate meridional gradients of PV along isentropic surfaces ($\partial_y P|_\Theta$, where subscript Θ indicates derivative at constant Θ, as opposed to derivatives at constant z, which are not indicated by a subscript). Concurrently, the mixing increases $\partial_y P|_\Theta$ at the tropopause [*Ambaum*, 1997; *Haynes et al.*, 2001]. The layer consisting of isentropes that cut the tropopause is often called middleworld, following [*Hoskins*, 1991]. Correspondingly, the layers consisting of isentropes that everywhere lie within the troposphere and stratosphere are called underworld and overworld, respectively. It is the strong PV gradients at the tropopause that make the dynamical tropopause definition meaningful, since they represent a barrier to (isentropic) mixing [*Haynes and Shuckburgh*, 2000]. However, there are sporadic events of breaking Rossby waves that strongly deform the tropopause and eventually lead to stratosphere-troposphere exchange (STE).

[7] STE has gained significant attention mainly because of its potential to alter the chemical composition of both tropospheric and stratospheric air (for a recent review on STE see *Stohl et al.* [2003]). However, local changes in the chemical composition within the tropopause region affect their radiative properties which represents a nonlocal effect (see *Shepherd* [2002] for a discussion). Studies on the chemical composition of the extratropical tropopause region have, e.g., focused on the so-called tropopause mixing layer, first described by *Dessler et al.* [1995] and recently further quantified by *Hoor et al.* [2004] and *Pan et al.* [2004], among others. This mixing layer lies just above the extratropical tropopause and exhibits chemical properties that are characteristic of both the troposphere and stratosphere. The existence of such a mixing layer suggests a persistent chemical impact of tropospheric processes on the lowermost extratropical stratosphere that is achieved by frequent troposphere-to-stratosphere exchange. A tropopause mixing layer might also suggest that the concept of a tropopause as interfacial surface between the troposphere and the stratosphere is in fact misleading and one should rather think of the tropopause as a transition layer between troposphere and stratosphere. However, it should be noted that this transition layer concept of the tropopause implies that individual STE events play a rather minor role since mixing takes place all the time in this concept and STE merely represents one segment of it. On the other hand, a mixing layer just above the extratropical tropopause might still form by individual, sporadic events exchanging mass between the troposphere and the stratosphere through an otherwise sharply defined tropopausal interface. Characteristics of such a mixing layer would then rather rely on local mixing on the stratospheric side of the tropopause and on the frequency of the sporadic STE events. In fact, one might argue that a sharp background tropopause is necessary for the tropopause mixing layer to be a stable, well-identifiable atmospheric feature. The question arises of how sharp the transition from troposphere to stratosphere is in long-term averages.

[8] A recent climatology based on vertically high resolved radiosonde data, $\mathcal{O}$(100 m), has addressed this question for two midlatitude sites located in southern Germany [*Birner et al.*, 2002]. A strong inversion at the tropopause in the mean vertical temperature gradient was uncovered; that is, temperature was found to strongly increase with altitude in the lowermost stratosphere. Consequentially, N^2 maximizes within this tropopause inversion layer (TIL hereafter) and the thermal tropopause is very sharp on average; that is, vertical STE is inhibited on average. The method of averaging the radiosonde profiles was crucial for these findings and is discussed in detail in section 2.

[9] The thermal structure of the TIL is not in agreement with conventional, textbook climatologies ($\mathcal{O}$(1 km) vertical resolution), who typically show about constant temperature within the midlatitude lower stratosphere (according to the U.S. standard atmosphere, USSA hereafter, see *NOAA/NASA/U.S. Air Force* [1976]). Furthermore, radiative equilibrium is in conflict with the thermal structure of the TIL, since it also yields about constant temperature within the midlatitude lower stratosphere [e.g., *Manabe and Wetherald*, 1967; *Thuburn and Craig*, 2002].

[10] How representative are the above results of southern Germany for the extratropics as a whole; that is, is the TIL a general extratropical feature and if yes, how do its characteristics depend on latitude? This question primarily stimulated the present study. Furthermore, a precise knowledge of the fine-scale structure of the entire extratropical tropopause region is important for a detailed understanding of STE, the radiative balance, but also, e.g., for estimating the wave-driving of the middle atmosphere (to the extend that the waves, Rossby and gravity, have to propagate through the tropopause region). High-resolution data sets have only become available in recent years. Amongst them, the data set stemming from 93 U.S.-operated radiosonde stations is, to the authors knowledge, the largest and most coherent one. These U.S. radiosonde stations cover a wide longitudinal and latitudinal range and, therefore, allow to answer the above question to a large extent. Five years (1998–2002) of data from the U.S. radiosonde station network are analyzed in the present study in order to explore the extratropical tropopause region. Thermal and wind structure as well as the resulting approximate PV structure are presented.

[11] The paper is organized as follows. In section 2, two different methods of averaging the radiosonde profiles are discussed. Section 3 describes the data set used in this study and methods that are applied. Results are presented in section 4, which includes climatologies for individual stations, zonally averaged climatologies divided into annual and seasonal means, and considerations of the midlatitude U.S. standard atmosphere. Finally, section 5 summarizes the results and discusses potential implications.

2. Conventional Versus Tropopause-Based Averaging

[12] Conventionally, the climate state is computed sea level based (SLB hereafter); that is, the vertical coordi-

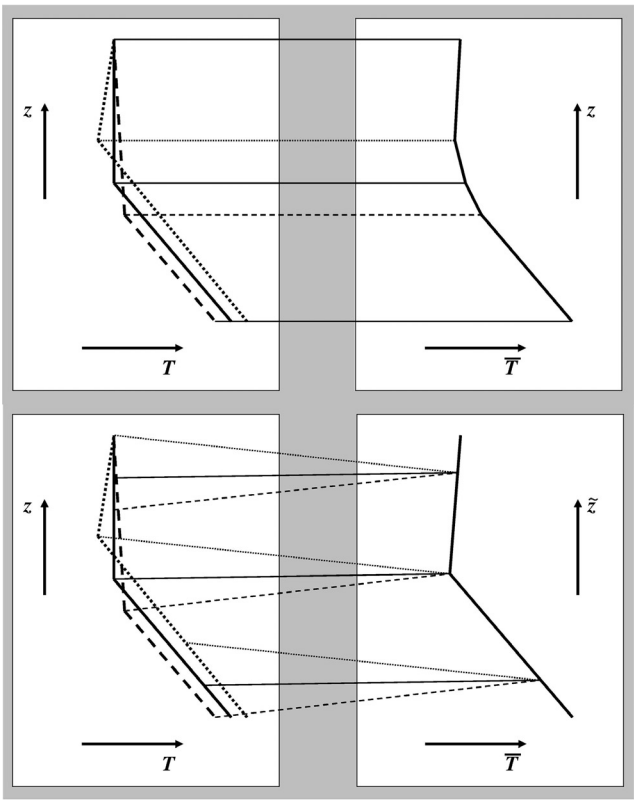

Figure 1. Schematic illustration of the two methods of averaging. (top) SLB average (conventional) and (bottom) TB average. (right) Temperature profile that results from averaging (left) three hypothetical temperature profiles. Each of the hypothetical profiles exhibits a sharp tropopause, though at different altitudes. Only the TB-averaged temperature profile preserves the sharp tropopause. See text for definition of $\tilde{z}$.

nate is fixed in time and horizontal space (for the time being, pressure-based coordinates can be considered to fall into this category). Any marked feature of the vertical structure that is strongly variable in time and horizontal space will be blurred in the resulting SLB climatology. This blur effect might be so strong that the marked feature becomes invisible in the climatology. An example of such an individually marked feature is the tropopause. At a given extratropical site the altitude of the tropopause (z_{TP}) fluctuates strongly in time. A typical range for z_{TP} in the extratropics is [5 km, 15 km]. This variability is mostly due to tropospheric synoptic-scale activity, i.e., weather. The vertical structure of meteorological quantities around the extratropical tropopause will thus be blurred in a conventional, SLB average. In order to preserve characteristic features coupled to the tropopause the average has to be computed with respect to the local, time-dependent altitude of the tropopause, i.e., tropopause-based (TB hereafter). That is, if $x(t, z)$ is a meteorological quantity of interest, then $\overline{x(t, z - z_{\mathrm{TP}}(t))}$ is the TB average of x, where the overbar denotes the time average. Once the TB average is computed the vertical coordinate can be readjusted by the time-averaged altitude of the tropopause $\overline{z_{\mathrm{TP}}}$:

$$\tilde{z} \equiv z - z_{\mathrm{TP}} + \overline{z_{\mathrm{TP}}}. \tag{1}$$

Note that while z is fixed in time with respect to the sea level, $\tilde{z}$ is fixed in time with respect to the tropopause. Figure 1 illustrates the differences between the two averages. In a climatology of the tropopause region the TB average clearly is advantageous compared to the SLB average.

3. Data and Methodology

[13] Vertically high resolved radiosonde data of 93 U.S.-operated stations of about twice-daily ascents are available for the years 1998–2002. To the authors knowledge this is the only freely available data set of high-resolution radiosoundings. It can be obtained at the SPARC data center (http://www.sparc.sunysb.edu). The same data set has been used previously by *Wang et al.* [2005] to study certain gravity wave characteristics. One can find a thorough description of the data set in the above paper (note especially the appendix on the data quality), as well as in [*National Climate Data Center* (*NCDC*), 1998]. Here only those characteristics of the data set that are essential for the present study are described.

[14] The radiosonde ascents provide near-vertical profiles of temperature, zonal and meridional wind components (u and v), relative humidity, and ascent rate as a function of pressure. The hypsometric equation is integrated in order to obtain z (strictly speaking z is geopotential height which is approximately equal to geometric altitude in the altitude range considered here). Only temperature and wind measurements are used in the present study (results on humidity are given by *Birner* [2003]). Generally, measurements are recorded every 6 seconds using the Microcomputer Automated Radio Theodolite (Micro-ART) system [*NCDC*, 1998] which leads to a vertical resolution of about 30 m given the typical ascent rate of $\approx$5 ms^{-1} of the radiosonde balloons. Wind data are estimated by tracking the balloon with the automated radio theodolite. This method can lead to spurious wind oscillations if the elevation angle of the balloon is very small. Therefore smoothing procedures had to be applied in order to reduce the noise of the wind data [cf. *NCDC*, 1998]. The resulting effective vertical resolution of the wind data is $\approx$150 m. *Wang et al.* [2005] note problems with the data quality in particular of the wind measurements. Similar to *Wang et al.* [2005] threshold criteria on the vertical wind shear are applied in order to remove suspiciously unphysical data. However, in contrast to *Wang et al.* [2005] the present study solely focuses on climate features; that is, only long-term averages of the profiles are considered. These long-term averages are certainly quite robust against individual spurious oscillations.

[15] Figure 2 shows the geographical distribution of the U.S. radiosonde stations. The longitudinal and latitudinal coverages of stations included in the present study (focusing on the extratropics) amounts to about [170°W, 70°W] and [24°N, 72°N], respectively. Emphasis here is on latitudinal structures. There are some gaps in the latitudinal coverage,

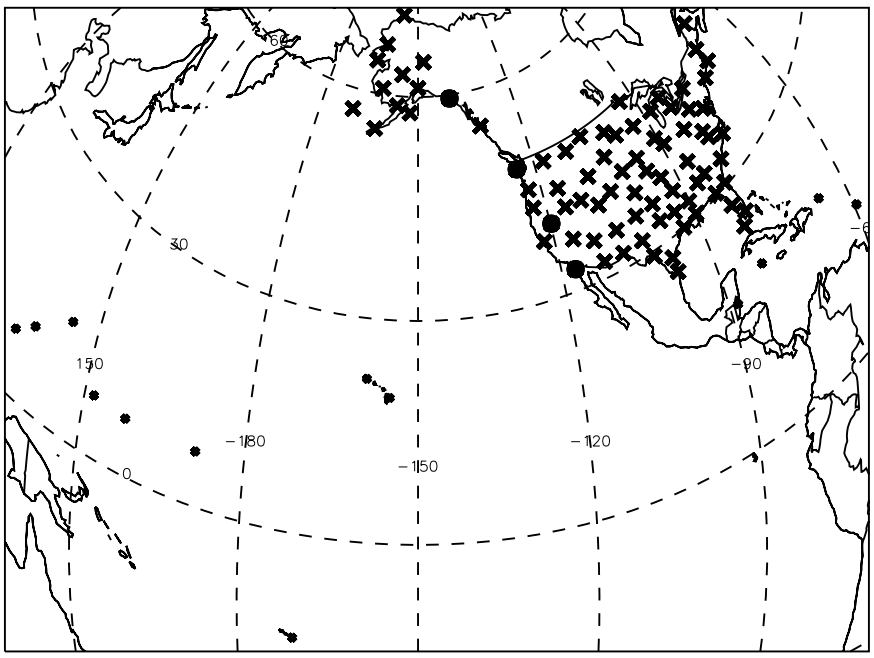

Figure 2. Geographical distribution of the U.S. radiosonde stations. Large crosses mark the stations included in the present study, small crosses mark excluded stations ("tropical," south of 24°N), and solid circles highlight stations used for individual climatologies.

most notably the range [49°N, 55°N] and north of about 72°N.

[16] As indicated in the previous section, two distinct methods of averaging the radiosonde profiles are considered in the present study. For the conventional, SLB average, data are interpolated on equidistant vertical levels using cubic splines. No coordinate transformation is applied for the SLB average as the vertical coordinate of individual soundings is already SLB. In contrast, for the TB average, the altitude of the thermal tropopause of each individual profile is computed first (as described in the appendix). Note that the thermal tropopause definition is the only applicable one for the present data set, since neither do the data provide ozone concentrations nor enough information in order to be able to compute reliable horizontal derivatives required to calculate PV.

[17] A modified vertical coordinate is defined as $z - z_{\mathrm{TP}}$ (which, with respect to sea level is dependent on time and location). Data are then interpolated on equidistant vertical levels in $z - z_{\mathrm{TP}}$, i.e., using the tropopause as a common reference level of all profiles within the average. That is, if $t = t_0$ denotes the profile's date, a given profile $x(t_0, z)$ is cubic spline interpolated on:

$$z_i(t_0) = z_{\mathrm{TP}}(t_0) + (i - K)\Delta z; \qquad i = i_{\min}(t_0), i_{\min}(t_0) + 1, \ldots, i_{\max}(t_0).$$

Here, K determines an arbitrary lower bound on $z_i(t_0)$ (in the present study $K = 12.9$ km/Δz); $i_{\min}(t_0)$ is the smallest i that fulfills $z_i \geq z_s$ (z_s denotes the radiosonde's station elevation); and $i_{\max}(t_0)$ is the largest i that fulfills $z_i \leq z_{\max}(t_0)$ ($z_{\max}(t_0)$ denotes the maximum altitude reached by the radiosonde balloon minus 500 m; profiles sometimes exhibit spurious fluctuations shortly before the burst of the balloon). The balloons typically reach maximum altitudes above 30 km, i.e., well above the region of interest in the present study (about 5–20 km). For temperature profiles $\Delta z = 50$ m, whereas for wind profiles $\Delta z = 150$ m. Only temperature (wind) data with less than 10 K (10 ms^{-1}) difference between consecutive levels and maximum level-spacing of 250 m (750 m) are considered. Finally, all available data of the interpolated profiles on each level i are averaged to form the TB-averaged profile. In all plots the modified vertical coordinate $\tilde{z}$ defined in equation (1) is employed.

[18] Zonal averages are obtained by latitudinally binning the radiosonde stations and subsequently averaging all individual climatologies within each latitude bin. However, since the stations are in general not equally distributed within a given latitude bin, a linear weighting function according to the stations meridional distances from the center of the latitude bin is applied to the zonal averages (the nearest neighbor latitude bins are included as well in order to obtain smooth meridional structures). A latitude binsize of 2° is used which leads to one major data gap between 50°N and 54°N and one minor data gap between 68°N and 70°N. Differences between averaged longitudes of stations south of 50°N and north of 54°N are quite large. Interpolation of data between 50°N and 54°N can thus lead to misinterpretations and is therefore avoided. However, a replacement of the minor data gap between 68°N and 70°N by interpolated data seems justifiable, because longitude differences between stations north and south of this minor data gap are small. As a result, there will be only one data gap between 50°N and 54°N in the zonal averages presented in section 4 (Figures 4–7 in section 4).

[19] Regarding wind climatologies, the horizontal wind speed $V = (u^2 + v^2)^{1/2}$ is evaluated instead of individual wind components for the following reasons. Wind clima-

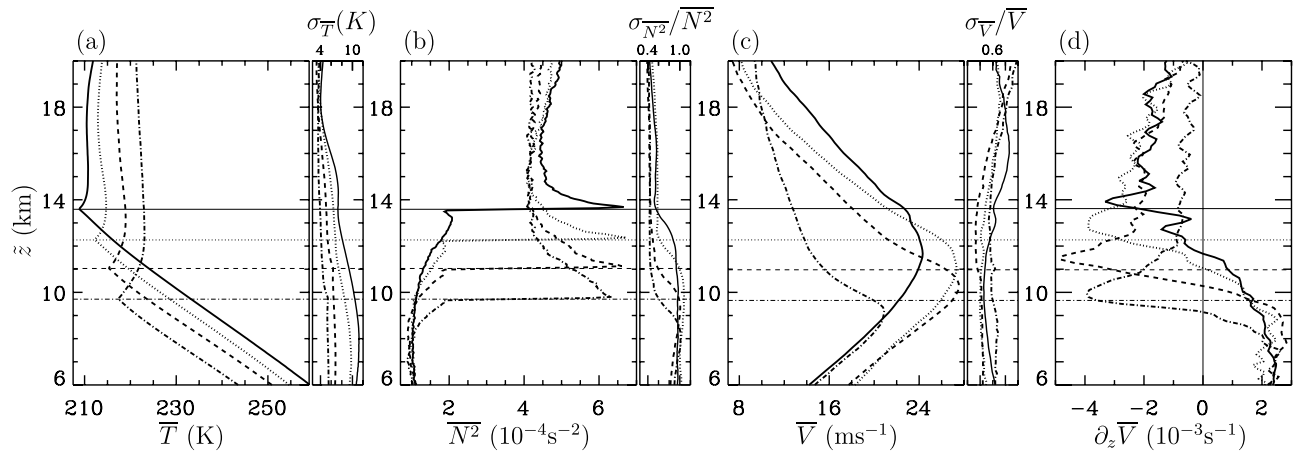

Figure 3. Annual TB climatologies and corresponding standard deviations (σ) of (a) temperature, (b) buoyancy frequency squared, (c) horizontal wind, and (d) vertical shear of the horizontal wind of the four stations: Miramar NAS, California (33°N, 117°W, solid); Reno, Nevada (40°N, 120°W, dotted); Quillayute, Washington (48°N, 125°W, dashed); and Yakutat, Alaska (60°N, 140°W, dash-dotted). Horizontal lines denote $\overline{z_{\mathrm{TP}}}$.

tologies of the extratropical tropopause region are dominated by jet stream signatures close to the tropopause. In long-term averages these jets are roughly oriented along latitude circles ($\overline{v} \approx 0$). However, individually, the jets are embedded into large-scale, say Rossby wave, disturbances, that meander around latitude circles (see, e.g., http://www.pa.op.dlr.de/arctic/ for daily updated wind maps on the tropopause). It follows that $\overline{u}$ is only representative of those parts of the jets that exhibit $v \approx 0$. In contrast, $\overline{V}$ is representative of the overall strength of the jets. Note, that this is, in its flavor, an equivalent latitude-like argument. The mean wind direction $\overline{\alpha}$ can be evaluated from $\tan\overline{\alpha} \equiv \overline{\sin\alpha}/\overline{\cos\alpha}$.

[20] In the results section the PV structure of the extratropical tropopause region is considered. Typically, $P = -g(f + \zeta_\Theta)(\partial_\Theta p)^{-1} = \rho^{-1}(f + \zeta_\Theta)\partial_z\Theta$, which is valid for hydrostatic flow [*Hoskins et al.*, 1985]. Here, f is the Coriolis parameter, ζ_Θ is relative vorticity evaluated on isentropic surfaces, and p is pressure. The radiosonde network is too sparse to reliably evaluate horizontal gradients (most of all ζ_Θ) required to compute individual PV fields. Nevertheless, one might consider the PV of the climatological mean flow. In long-term averages ζ_Θ typically is one order of magnitude smaller than f (equivalent to assuming small Rossby number $\epsilon \equiv |\zeta_\Theta/f|$). The so-called planetary approximation of PV neglects the contribution due to ζ_Θ:

$$P_{\mathrm{plan}} \equiv \rho^{-1} f \partial_z \Theta, \tag{2}$$

and can therefore be interpreted as representing the leading order contribution to PV for small Rossby number (note $P = (1 + \zeta_\Theta/f)P_{\mathrm{plan}}$). Only vertical information is required to evaluate P_{plan}; that is, it can be obtained in high resolution from the available data. The $\mathcal{O}(\epsilon)$-correction to PV is estimated from the zonally averaged climatological wind structure. It is:

$$\overline{\zeta_\Theta} \approx \tilde{\zeta}_\Theta \equiv -(a\cos\varphi)^{-1}\partial_\varphi(\tilde{u}\cos\varphi)|_\Theta, \tag{3}$$

where $\tilde{u} \equiv -\overline{V}\sin\overline{\alpha}$, a is Earth's radius, and φ is latitude (note $\partial_\varphi|_\Theta = \partial_\varphi + s\partial_z$, where $s = -\partial_y\Theta/\partial_z\Theta$ is the meridional slope of isentropes). Therefore

$$\tilde{P} \equiv \overline{\rho}^{-1}\left(f + \tilde{\zeta}_\Theta\right)\partial_z\overline{\Theta} \tag{4}$$

is considered as approximated PV of the zonally averaged climatological mean flow. Note, however, that the latitudinal resolution of the present data set is much coarser than its vertical resolution. As a consequence the barotropic structure of the flow is somewhat underrepresented compared to its baroclinic structure.

[21] It should be noted that there is generally a difference between averaged PV and PV computed from averaged fields. The main shortcoming of the elaborations above is the correlation that exists on average between ζ_Θ and $\partial_z\Theta$ [cf. *Zängl and Wirth*, 2002; *Wirth*, 2003] which is not included in the current approach. Nevertheless, the contribution due to this correlation can be discussed qualitatively (see section 5).

4. Results

[22] The focus of this paper is on the thermal and wind structure of the extratropical tropopause region, which both can be derived directly from the available data. Additionally, the approximated PV structure is examined, which is of dynamical interest and can be evaluated from the averaged thermal and wind structures. In this regard, it has been noted as early as in the original paper by *Ertel* [1942] that Θ can be replaced by any function of Θ in the definition of PV without losing its conservation properties. That is, the vertical structure of PV is arbitrary to some extent. In the stratospheric community, e.g., it is common practice to redefine PV such that its strong increase with altitude due to $1/\rho$ is counterbalanced by a certain modifying factor, which is a function of Θ alone [e.g., *Müller and Günther*, 2003]. This is useful in vertical cross sections of PV, in which the (arbitrary) vertical structure of P would over-

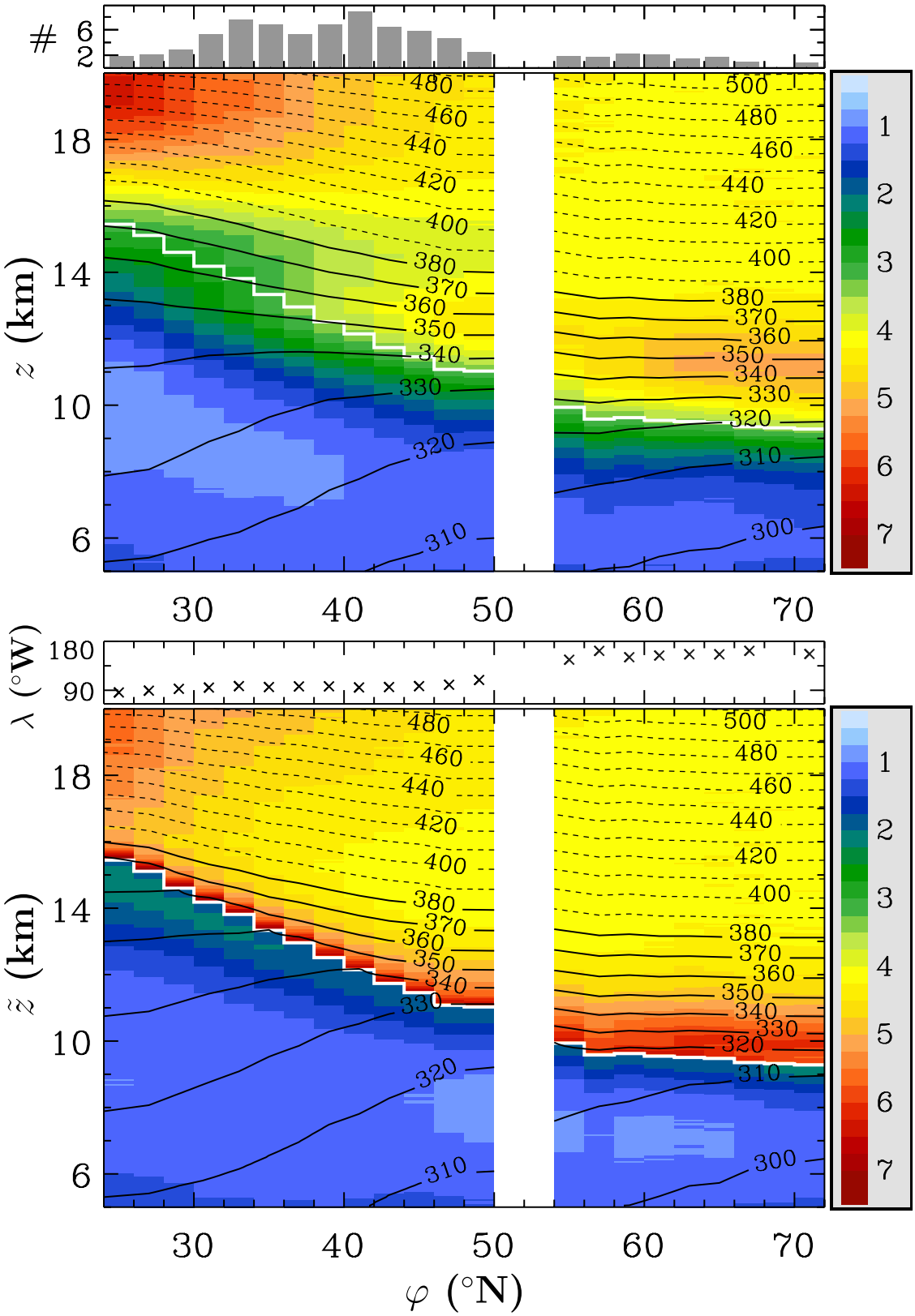

Figure 4. Zonally averaged climatological annual mean N^2 (10^{-4} s^{-2}, color shading) and Θ (K, contours, overworld dashed) as a function of latitude and altitude. (top) SLB average (conventional) and (bottom) TB average (note modified altitude). Thick white lines denote $\overline{z_{TP}}$. White areas represent data gaps. The top parts of the diagrams show per latitude bin: the number (#) of available stations (Figure 4, top) and the average longitude λ at tropopause level (Figure 4, bottom).

whelm the overall structure (most importantly the dynamically relevant quasi-horizontal structure along isentropes). Therefore, in the cross sections shown in the present paper, the function $(\overline{\Theta}/300\mathrm{K})^{-3.5}\,\tilde{P}$ is plotted instead of $\tilde{P}$.

4.1. Individual Stations

[23] We first focus on four individual stations separated by about 10° in latitude with similar longitudes (along the west coast of North America): Miramar NAS, California (33°N, 117°W), Reno, Nevada (40°N, 120°W), Quillayute, Washington (48°N, 125°W), and Yakutat, Alaska (60°N, 140°W). Figure 3 shows TB-averaged climatological profiles of temperature, buoyancy frequency squared, horizontal wind, and vertical shear of the horizontal wind for these four stations. Despite substantial differences in their tropopause characteristics, a TIL exists at all four stations: T strongly increases just above the tropopause which is associated with a sharp maximum in N^2. The thickness of the TIL increases toward the pole (from about 500 m at 33°N to about 3 km at 60°N). At 48°N the TIL is about 2 km thick, which corresponds to the value for Munich [*Birner et al.*, 2002], also located at 48°N, but at a very different longitude. All four stations show a similar almost discontinuous jump in N^2 at the tropopause; that is, on average the tropopause constitutes a very sharp interface. Outside of the TIL, N^2 is rather constant and assumes typical tropospheric and stratospheric values, respectively.

[24] Jet stream signatures with maximum wind speeds close to the tropopause exist in all $\overline{V}$ profiles. The latitude of the subtropical jet strongly varies with season (see below) such that the station at 33°N is located close to the jet core in winter but south of the jet in summer. That is, tropopause characteristics are rather of tropical nature in summer for this station. This strong dependency on season affects the structure of meteorological quantities around the tropopause in the overall mean (see *Birner* [2003] for further details). Characteristics of the profiles at 60°N are affected by the quasi-stationary ridge over Alaska (a.k.a. the Aleutian high). Accordingly, the mean wind direction exhibits a southerly component leading to mean southwesterlies throughout the plotted altitude range (not shown). The other three stations exhibit westerlies throughout the plotted altitude range.

[25] A sharp minimum in $\partial_z\overline{V}$, that approximately coincides with the maximum in N^2, appears just above the tropopause at all four stations. Outside of the TIL, $\partial_z\overline{V}$ is rather constant. It follows that the TIL represents a distinct layer in both the thermal and wind structure for all four stations.

4.2. Zonal Averages: Annual Mean

[26] In this section data from all stations north of 24°N are used in order to obtain a zonally averaged climatological annual mean fine-scale picture of the extratropical tropopause region. Thermal, wind, and approximated PV structure are considered.

4.2.1. Thermal Structure

[27] Figure 4 shows zonally averaged cross sections of climatological annual mean N^2 and Θ, SLB (conventional, top) and TB averaged (bottom), respectively. The latitude bin centered at 69°N does not contain any station, however, interpolated data have been used to fill the gap (see section 3).

[28] The SLB climatology serves as a high-resolution version of previous climatologies and is described first. Tropospheric values of N^2 center around $1 \cdot 10^{-4}\ \mathrm{s}^{-2}$ with very small variations in latitude and altitude. Stratospheric values of N^2 center around $7 \cdot 10^{-4}\ \mathrm{s}^{-2}$ at the tropical edge of the plotted latitude range and around $4.5 \cdot 10^{-4}\ \mathrm{s}^{-2}$ in the extratropics. The transition from tropospheric to stratospheric values of N^2 is rather smooth, particularly between about 25°N and 35°N. Only the polar regions show slightly enhanced values of N^2 just above the tropopause, a slight indication of a TIL. Middleworld isentropes show a smooth transition from positive tropospheric to negative stratospheric slopes in the extratropics. All in all, the SLB climatology does not differ significantly from previous climatologies [e.g., *Peixoto and Oort*, 1992].

[29] The TB climatology differs quite substantially from the conventional one in the extratropical tropopause region. Here, the tropopause shows up as a very sharp interface between troposphere and stratosphere throughout the extratropics, as suggested by the TB-averaged climatologies of individual stations. Figure 4 furthermore shows the existence of the layer of enhanced values of N^2 just above the tropopause (the TIL) in the entire extratropical latitude range. This is the main result of this paper and substantially generalizes the findings of [*Birner et al.*, 2002] to a much wider range of longitudes and latitudes. The thickness of the TIL increases toward the pole. However, the TIL resides within the lowermost stratosphere for all latitudes, i.e., within the stratospheric part of the middleworld (below Θ = 380 K). Maximum values of N^2 exceed $6 \cdot 10^{-4}\ \mathrm{s}^{-2}$ at all latitudes. Middleworld isentropes show a kink at the tropopause in contrast to the conventional climatology. Outside of the extratropical tropopause region the TB climatology does not differ much from the conventional climatology.

4.2.2. Wind Structure

[30] Figure 5 shows zonally averaged cross sections of climatological annual mean $\partial_z V$ and V, SLB (conventional, left) and TB averaged (right), respectively.

[31] The bulk of the extratropical troposphere is characterized by positive vertical wind shear with values between $2 \cdot 10^{-3}\ \mathrm{s}^{-1}$ and $3 \cdot 10^{-3}\ \mathrm{s}^{-1}$ in both the conventional and TB climatology. In the extratropical lower stratosphere, however, the two methods of averaging yield significantly different results. The conventional climatology shows broadly distributed negative values of $\partial_z\overline{V}$ in the lower stratosphere, whereas in the TB climatology, $\partial_z\overline{V}$ has a distinct minimum (values around $-4 \cdot 10^{-3}\ \mathrm{s}^{-1}$) just above the tropopause throughout most of the extratropics. Maximum wind speeds are located slightly below the tropopause with the overall jet maximum located at about 45°N ($\overline{V}_{\max} \approx 30\ \mathrm{ms}^{-1}$). This jet maximum represents the entrance region of the Atlantic storm track at the east coast of North America. Differences between the conventional and the TB climatology are less obvious in $\overline{V}$.

[32] The mean wind direction (not shown) is westerly in the bulk of the extratropics with very small variations in altitude. Only the subpolar region of our study (Alaska)

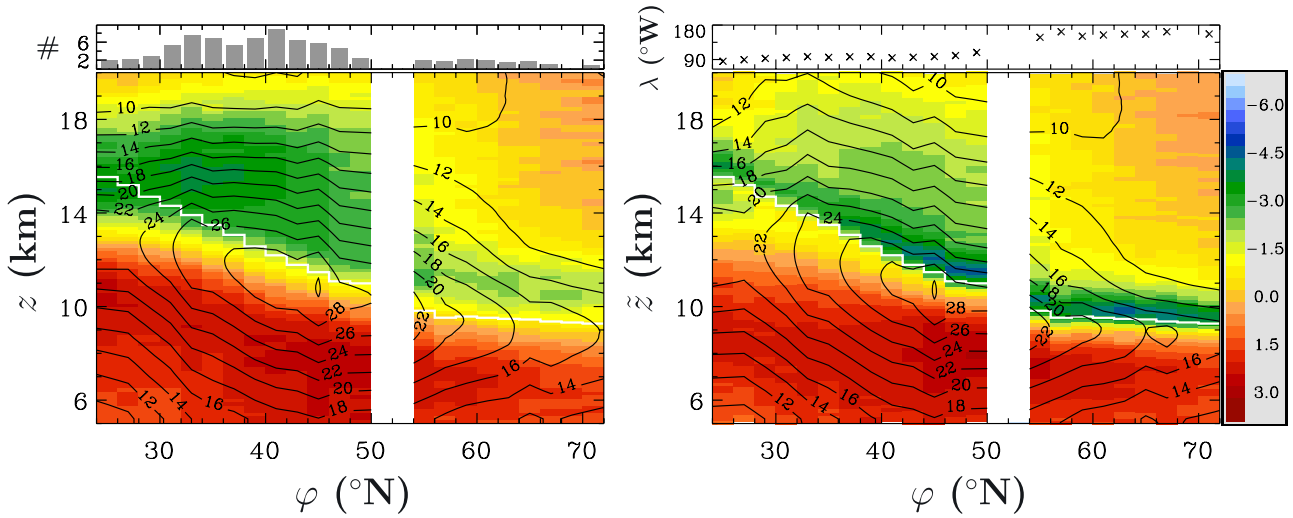

Figure 5. As Figure 4 but for V (ms^{-1}, contours) and its vertical derivative $\partial_z \overline{V}$ (10^{-3} s^{-1}, color shading). (left) SLB averages and (right) TB averages.

exhibits southerly components throughout the analyzed altitude range.

4.2.3. PV Structure

[33] Figure 6 shows cross sections of $(\overline{\Theta}/300\text{K})^{-3.5}\,\tilde{P}$ and $\overline{\Theta}$. Zonally averaged annual SLB (conventional, left) and TB climatologies (right) of T, Θ, and V were used to calculate $\tilde{P}$ from equation (4). Of interest is the PV distribution along isentropes, which is qualitatively independent on the modifying factor used in the plots. We will therefore simply refer to $\tilde{P}$ in the following.

[34] First, the conventional average is discussed. All middleworld isentropes are characterized by smoothly increasing $\tilde{P}$ toward the pole. $\partial_y \tilde{P}|_\Theta$ is somewhat enhanced around the tropopause and somewhat reduced within the troposphere far away from the tropopause. The turbulent nature of the troposphere does not show up very clearly and the tropopause is not very distinct. Within the stratosphere, $\tilde{P}$ increases with latitude because of f, which suggests that dynamics have only a minor impact on the averaged PV structure there.

[35] In the TB climatology, on the other hand, $\tilde{P}$ exhibits a very sharp tropopause (contours corresponding to values of $\tilde{P}$ between about 2.5 PVU and 6 PVU are all covered by the white line denoting the tropopause). The large maximum values of $\partial_y \tilde{P}|_\Theta$ at the tropopause indicate a strong isentropic mixing barrier. Within the troposphere $\tilde{P}$ is rather constant; that is, $\partial_y \tilde{P}|_\Theta$ is rather small, indicating frequent turbulent mixing. Within the TIL $\tilde{P}$ is rather constant as well (contours of $\overline{\Theta}$ and $\tilde{P}$ run roughly parallel). This might be a surprising result; the smallness of $\partial_y P|_\Theta$ is typically associated with tropospheric dynamics, whereas the TIL resides within the lowermost stratosphere. The extratropical tropopause might therefore be interpreted as representing the interface between two rather well-mixed layers: the tropo-

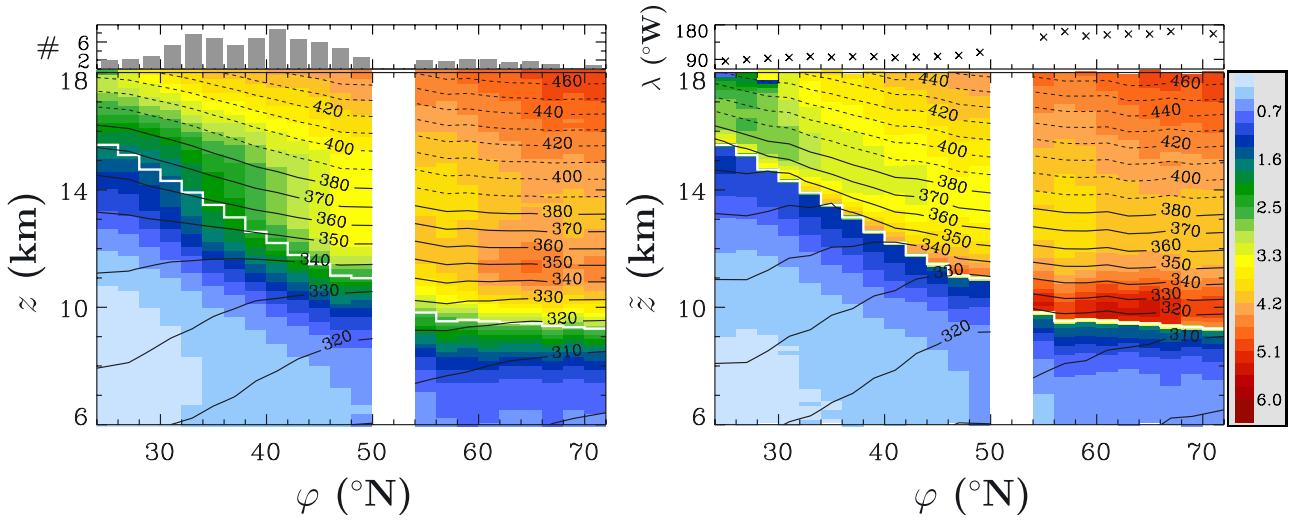

Figure 6. As Figure 4 but for $(\overline{\Theta}/300\text{K})^{-3.5}\,\tilde{P}$ (in PVU, color shading, note logarithmic scale) computed from climatological annual mean thermal and wind structure. (left) SLB and (right) TB. Isentropes (contours) are equal to those in Figure 4.

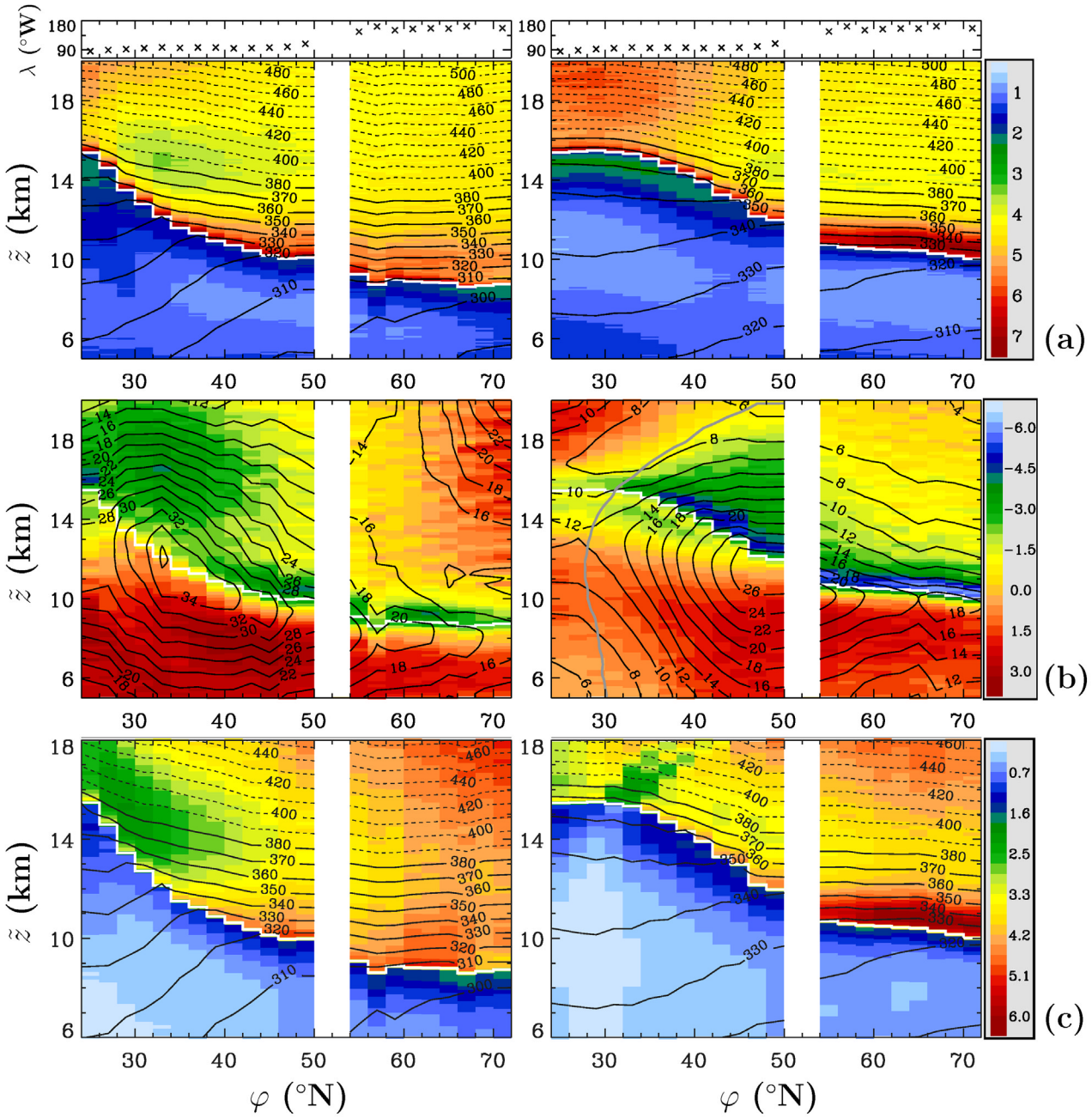

Figure 7. Zonally averaged climatological seasonal TB mean for (left) winter (December–January–February) and (right) summer (June–July–August). (a) N^2 (10^{-4} s^{-2}, color shading) and Θ (K, contours); (b) $\partial_z V$ (10^{-3} s^{-1}, color shading) and V (ms^{-1}, contours), gray line depicts the wind reversal in summer; and (c) $\tilde{P}$ (PVU, color shading) and Θ (K, contours, as in Figure 7a). Thick white lines, white areas, and top parts of the diagrams in Figure 7a as in Figure 4.

sphere and the TIL. Note that the cyclonic shear just north of the tropopause is most likely underestimated, as is the anticyclonic shear just south of the tropopause, because of the coarse latitudinal resolution in the present data set. That is, $\partial_y P|_\Theta$ is most likely even smaller than $\partial_y \tilde{P}|_\Theta$ within both the troposphere and the TIL. Note further that we generally find $\epsilon < 0.1$ (not shown, compare equation (4)); that is, the PV structure is dominated by the planetary contribution P_{plan}.

[36] On overworld isentropes (above 380 K) $\tilde{P}$ steadily increases with latitude as in the SLB climatology (contours of $\tilde{P}$ are more steeply sloped than contours of $\overline{\Theta}$ within the overworld in Figure 6).

4.3. Zonal Averages: Winter-Summer Contrast

[37] Figure 7 shows zonally averaged cross sections of the climatological seasonal TB mean thermal, wind, and approximated PV structure divided into winter (DJF) and summer (JJA).

[38] Characteristics of the meridional structure of the tropopause itself are quite different between winter and summer: tropical and subpolar $\overline{z_{\text{TP}}}$ differ by about 8.5 km

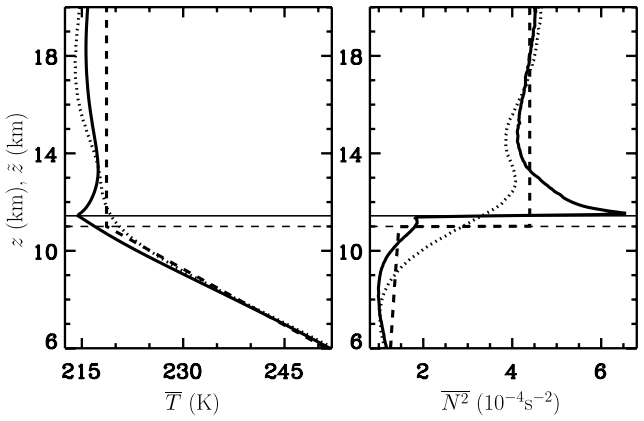

Figure 8. Averaged profiles representative of about 45°N of (left) temperature and (right) buoyancy frequency squared. All stations within the latitude range [41.5°N, 49°N] are included. Dotted lines indicate SLB average, solid lines indicate TB average, and dashed lines indicate profiles of the USSA at 45°N. Horizontal lines denote $\overline{z_{TP}}$.

in winter and by about 6 km in summer. Accordingly, the magnitude of the meridional slope of the tropopause ($|\partial_y \overline{z_{TP}}|$) at its maximum location is about twice as large in winter ($\approx 4 \cdot 10^{-3}$ at about 30°N) than in summer ($\approx 2 \cdot 10^{-3}$ at about 45°N).

[39] The thermal structure of the TIL exhibits a remarkable seasonal variation, in contrast to most of the thermal structure outside of the TIL. In winter, the meridional and vertical extent of the TIL (i.e., its volume) is much larger than in summer. On the other hand, values of N^2 in the summer TIL exceed those of the winter TIL by a factor of about 1.5. This distinct difference between winter and summer is referred to as the winter-summer contrast. Outside of the extratropical tropopause region, differences between winter and summer are rather small. It should be remarked that in winter there exists a region (between about 14–16 km and 28°N–40°N) with somewhat reduced values of N^2 (see also SLB climatology in Figure 4). This indicates the frequent existence of a secondary tropopause with rather tropical/subtropical characteristics. A close analysis of this feature is the subject of current investigation and will be published elsewhere.

[40] The wind structure in the extratropical tropopause region largely reflects thermal wind balance (see discussion in section 5). In winter, the maximum wind speed exceeds 36 ms^{-1}, whereas in summer it is smaller by about 10 ms^{-1}. Accordingly, wind shear values in the troposphere are larger in winter (around $3 \cdot 10^{-3}$ s^{-1}) than in summer (around $2 \cdot 10^{-3}$ s^{-1}). In the TIL, on the other hand, the minimum in $\partial_{\tilde{z}} \overline{V}$ is much more pronounced in summer ($<-5 \cdot 10^{-3}$ s^{-1}) than in winter ($\approx -3 \cdot 10^{-3}$ s^{-1}), which is a similar behavior to N^2 within the TIL. Note that the wind speed rather peaks right at the tropopause in winter, whereas it peaks slightly below the tropopause in summer (as is evident in the thermal structure taking into account the thermal wind relation: $\partial_z u \propto -\partial_y \Theta$). Therefore the wind-speed peaks slightly below the tropopause in the overall mean as well (Figure 5). The wind direction (not shown) is westerly with very small variations for the regions of strong winds around the jet maxima in both winter and summer. In summer, the wind reverses to easterlies within the lower extratropical stratosphere. The subpolar region within the present study (Alaska) exhibits southwesterly winds in both winter and summer.

[41] $\tilde{P}$ is rather well mixed within the troposphere in both winter and summer, though it exhibits somewhat enhanced values just below the tropopause. Within the overworld (above Θ = 380 K) $\tilde{P}$ steadily increases with latitude according to f, except for latitudes within about [40°N, 50°N] in summer where $\tilde{P}$ is roughly constant along isentropes with a strong gradient south of this latitude range. This strong gradient is due to the stratospheric wind reversal in summer (depicted as gray line in Figure 7b). Within the TIL $\tilde{P}$ is roughly constant along isentropes (contours of $\overline{\Theta}$ and $\tilde{P}$ run roughly parallel). Therefore, in both winter and summer the extratropical tropopause can be viewed as separating two well-mixed layers: the troposphere and the TIL.

4.4. Standard Atmosphere

[42] The temperature profile of the USSA is widely used as a background atmosphere, especially in idealized studies, even though it was constructed about 40 years ago. Results shown thus far, however, suggest a modification of the USSA around the tropopause. The aim of this section is therefore to provide a representative fine-scale reference atmosphere of the midlatitude tropopause region by means of T and N^2.

[43] The midlatitude temperature profile of the USSA is meant to be representative for 45°N. In order to average profiles representative for 45°N data from all stations with latitudes between [41.5°N, 49°N] are used, which gives an average latitude of 44.96°N, very close to 45°N. Overall, 21 stations fall into this latitude range.

[44] Figure 8 shows climatological profiles of T and N^2 comparing TB and SLB averages, as well as the USSA. Not surprisingly (bearing the results thus far in mind), there appear large differences between the SLB and TB climatologies in particular around the tropopause. As in the individual station's climatologies, the TB-averaged profiles exhibit a TIL. The SLB-averaged N^2 profile appears as a smoothed version of the USSA N^2 profile and lacks a well-defined tropopause. It becomes clear that the step-like transition in the USSA N^2 profile is certainly not representative of the actual behavior of N^2 at and just above the tropopause, as captured by the TB average. Furthermore, a strong increase in temperature just above the tropopause in the TB climatology replaces the isothermal behavior of the USSA. All in all, it is mainly the TIL where the USSA does not appear to be representative of the actual thermal structure which emerges in the TB climatology.

5. Discussion

[45] The vertical structure of the TIL is characterized by extrema in the vertical gradients of temperature and wind. Thermal and wind structure are typically not independent of each other. One expects, e.g., the thermal wind relation to hold in long-term averages. Consider a purely zonal wind; that is, V is equal to the zonal wind

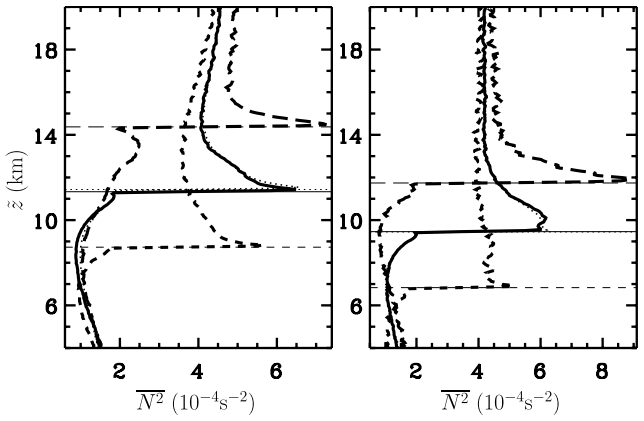

Figure 9. TB-averaged (left) midlatitude (all stations within [41.5°N, 49°N]) and (right) subpolar (all stations with $\varphi > 60°$N) profiles of buoyancy frequency squared divided into different strength of tropopause anomaly z'_{TP} (defined as difference of individual z_{TP} from monthly climatology). Solid lines indicate -0.5 km $\leq z'_{\mathrm{TP}} < 0.5$ km (near-zero anomalies), long-dashed lines indicate $z'_{\mathrm{TP}} \geq 2$ km (strong anticyclonic anomalies), short-dashed lines indicate $z'_{\mathrm{TP}} < -2$ km (strong cyclonic anomalies), and thin dotted lines indicate overall average (i.e., thin dotted line on left is equal to solid line in Figure 8 (right)). Horizontal lines denote corresponding $\overline{z_{\mathrm{TP}}}$. Note different abscissa scales.

component u. The thermal wind relation in u is approximately given by

$$\partial_z u = -g(f\Theta)^{-1}\partial_y \Theta,$$

(the term proportional to $\partial_y p$ has been neglected). Differentiating by z leads to

$$\partial_z(\partial_z u) \equiv \partial_{zz} u = -\frac{1}{f}\partial_y N^2. \tag{5}$$

It follows that an extremum in N^2 along y (i.e., $\partial_y N^2 = 0$) is associated with an extremum in $\partial_z u$ along z (i.e., $\partial_{zz} u = 0$). An inspection of Figure 4 yields that the maximum in N^2 just above the tropopause represents a maximum along y just north of the tropopause at the same time. This is due to the fact that the tropopause has a meridional slope. Therefore, after equation (5), $\partial_z u$ extremizes where N^2 has its maximum (just above the tropopause). Furthermore, relation (5) is invariant against rotation along z. The above arguments thus equally apply to the mean horizontal wind if y is replaced by the horizontal coordinate normal to the mean wind direction. Therefore the observed coexistence of the extrema in N^2 and $\partial_z V$ just above the tropopause merely represents thermal wind balance. Note that (5) does not provide a quantitative relation between the strength of the two extrema.

[46] PV as approximated by equation (4) is rather well-mixed within the extratropical troposphere and the TIL. What are the modifications due to the neglected correlation between ζ_Θ and $\partial_z\Theta$ in the "full" PV ($\overline{P} = \tilde{P} + \overline{P'_{\mathrm{plan}}\zeta'_\Theta}/f \approx \tilde{P} + \overline{\rho^{-1}\partial_z\Theta'\zeta'_\Theta}$, see section 3)?

[47] PV inversion can be used to study upper tropospheric balanced disturbances [see *Hoskins et al.*, 1985; *Thorpe*, 1986; *Wirth*, 2003]. It has been shown that anticyclonic balanced disturbances ($\zeta'_\Theta < 0$) lead to a higher and sharper tropopause; that is, N^2 is enhanced just above the tropopause (but also somewhat enhanced just below the tropopause, see *Wirth* [2003]). Conversely, cyclonic balanced disturbances ($\zeta'_\Theta > 0$) lead to a lower and less sharp tropopause; that is, N^2 is reduced just above the tropopause (and slightly reduced just below it as well). The associated changes in the thermal structure can be interpreted as being achieved by the secondary circulations accompanying the tropopause disturbances [*Wirth*, 2004]. It follows that there is a negative correlation between ζ_Θ and N^2 (or $\partial_z\Theta$), see also *Zängl and Wirth* [2002]. This negative correlation reduces the well-mixed behavior of PV on average.

[48] The data set used in the present study does not allow the computation of individual ζ_Θ perturbations. However, as noted above there is a negative correlation between upper tropospheric ζ'_Θ and anomalies in tropopause altitude (z'_{TP}, tropopause anomalies for short in the following). It is therefore useful to explore the thermal structure of the extratropical tropopause region as a function of tropopause anomaly z'_{TP}. Of interest here are the midlatitude and subpolar regions of the data set. Figure 9 shows TB-averaged climatological profiles of N^2 divided into different z'_{TP} for midlatitudes (40–50°N) and subpolar latitudes ($\varphi >$ 60°N), respectively. Indeed, as noted above, negative tropopause anomalies are associated with reduced values and positive tropopause anomalies are associated with enhanced values of N^2 just above the tropopause. However, except for very strong negative z'_{TP} the existence of the maximum in N^2 just above the tropopause is independent of the sign and strength of z'_{TP}. In fact, the vertical structure of N^2 at $z'_{\mathrm{TP}} \approx$ 0 is very similar to that of the overall average. That is, the correlation between ζ_Θ and N^2 does not seem to affect much the structure of the "full" PV. This furthermore strengthens our hypothesis that the PV is rather well-mixed within the troposphere and the TIL.

[49] PV mixing over large distances is achieved by irreversible stirring due to large-scale dynamics. These large-scale dynamics can be parameterized to some degree by so-called eddy diffusivities (see *Schneider* [2004] for a discussion). The assumption hereby is that large-scale eddies behave as (macro-)diffusion, which is useful when considering the net effect of the eddies on the long-term mean flow. In terms of heat fluxes such a parameterization reads

$$\overline{v'T'} = -\mathcal{D}\partial_y\overline{T}, \tag{6}$$

where the primes denote deviations from the mean (the eddies) and $\mathcal{D}$ is an eddy diffusivity. Here, relation (6) is used solely to estimate the sign of the heat flux and related quantities.

[50] In the troposphere $\partial_y T < 0$ such that large-scale eddies lead to a poleward heat flux based on (6) [e.g., *Peixoto and Oort*, 1992]). In the TIL, however, $\partial_y T > 0$ such that large-scale eddies, if present, lead to an equatorward heat flux based on (6). On the other hand, the lower stratosphere above the TIL cannot be described as well

mixed on average (Figure 6); that is, dynamics has a minor impact on the average thermal structure and temperatures are expected to be closer to radiative equilibrium temperatures. Radiative equilibrium in midlatitudes yields about constant temperature with altitude in the lower stratosphere [e.g., *Manabe and Wetherald*, 1967]. As a result heat fluxes of the kind described by (6) should lead to a relative warming in the midlatitude TIL. In fact, the dynamical heating due to horizontal dynamics is proportional to $\partial_y \overline{v'T'} \sim -\partial_{yy}\overline{T} \sim \partial_{yz}\overline{u}$, where the last step assumes thermal wind balance. An inspection of Figure 5 yields $\partial_{yz}\overline{u} > 0$ on average in the TIL, i.e., dynamical warming. This seems to provide a possible explanation of the local temperature maximum just above the tropopause in midlatitudes. The temperature minimum at the tropopause is then produced by the dynamical warming in the TIL combined with large-scale eddy mixing in the troposphere which tends to raise and therefore cool the tropopause [e.g., *Egger*, 1995].

[51] Characteristics of the TIL exhibit a striking seasonal variation (referred to as winter-summer contrast). Properties of the extratropical tropopause itself show strong seasonal variations: much higher tropopauses in summer compared to winter in the subpolar regions and a much stronger meridional tropopause slope in winter compared to summer in midlatitudes. This winter-summer contrast in tropopause properties is associated with the seasonal variation of the strength and meridional position of the jet stream: the jet stream is considerably weaker and located further poleward in summer compared to winter. The associated hemispheric cyclonic circulation is much weaker in summer than in winter. A weakened cyclonic circulation can be interpreted as a relative anticyclonic perturbation (here of hemispheric scale). As noted above, upper tropospheric anticyclonic perturbations are associated with an elevated tropopause and enhanced values of N^2 just above the tropopause (see also Figure 9). It is thus hypothesized here that the enhanced values of N^2 in the summer TIL compared to winter are caused by the hemispheric relative anticyclonic perturbation of the jet stream. This represents a possible explanation of the winter-summer contrast. Note that any explanation of the winter-summer contrast does not provide an explanation of the existence of the TIL.

6. Summary and Implications

[52] The main results of this study can be summarized as follows. Conventional, i.e., SLB averages yield a blurred vertical structure of meteorological quantities around the extratropical tropopause. This is due to the large variability, in time and space, of the tropopause altitude at extratropical latitudes. The TB average circumvents this problem by using the tropopause as a common reference level of all vertical profiles within the mean. A strong inversion at the extratropical tropopause in the vertical temperature gradient is uncovered by the TB average; that is, temperature strongly increases with altitude just above the extratropical tropopause. A distinct maximum in the static stability parameter N^2 is associated with this temperature increase, above which N^2 decays roughly exponentially toward typical stratospheric values. This tropopause inversion layer (TIL) exists on average throughout the investigated extratropics, i.e., on a wide range of longitudes and latitudes. This constitutes the main result of this paper and substantially generalizes the previous result, representative of southern Germany only [*Birner et al.*, 2002]. It can be concluded that the TIL seems to be a general extratropical phenomenon, although more evidence from other regions is still required.

[53] The thickness of the TIL increases toward the pole from about 500 m at the tropical edge to about 3 km at 72°N in the annual mean. Properties of the TIL exhibit a strong contrast between winter and summer. In winter the volume of the TIL is much larger than in summer whereas values of N^2 in the TIL are much larger in summer than in winter. The TIL exhibits a distinct wind structure. A strong minimum in $\partial_z V$ exists just above the extratropical tropopause which approximately coincides with the maximum in N^2. In terms of approximated PV ($\tilde{P}$) the TIL is rather well mixed. Since generally $\epsilon < 0.1$, this well-mixed $\tilde{P}$ is mainly due to the planetary contribution P_{plan} (compare equation (4)). This in turn implies that mainly horizontal and vertical structures of $N^2 \propto \partial_z \Theta$ are responsible for the well-mixed PV. The importance of horizontal structure in N^2 (i.e., vertical structure in baroclinicity) is often underestimated, especially in theoretical studies on large-scale dynamics.

[54] Well-mixed PV in the TIL suggests large-scale dynamics to take place sufficiently frequently in the TIL and therefore in large parts of the lowermost stratosphere. The vertical resolution required to resolve such dynamics in the TIL can be estimated as follows. A typical aspect ratio (horizontal to vertical scale) of large-scale dynamics is given by N/f. In the midlatitude troposphere $N/f \sim 100$ such that a synoptic weather system of $\mathcal{O}(1000$ km) might require a horizontal resolution of 100 km yielding a required vertical resolution of 1 km. In the midlatitude TIL, however, $N/f \sim 250$ such that a vertical resolution of 400 m is required to fit a horizontal resolution of 100 km. It follows that typical forecast models should have problems representing dynamics in the extratropical tropopause region. For example the ECMWF model, a state of the art operational global forecasting model, currently runs with about 800 m vertical resolution in the extratropical tropopause region yet about 40 km horizontal resolution (T511 [*Untch et al.*, 1999]) which does not seem to be consistent with the aspect ratio of the dynamics in the extratropical tropopause region. Note that *Birner et al.* [2002] noticed the absence of a TIL in ECMWF reanalysis data over southern Germany. Furthermore, a recent analysis of the vertical structure of forecast errors has revealed maximum errors around the midlatitude tropopause [*Hakim*, 2005]. The above caveats strongly suggest the use of a finer vertical resolution in the extratropical tropopause region in weather forecast models. The results by *Wittman et al.* [2004] that the lower stratospheric shear can substantially influence baroclinic wave life cycles in the troposphere furthermore strengthens the above argument. It is interesting to note that the issue of consistent horizontal and vertical resolution in numerical models is not new [*Lindzen and Fox-Rabinovitz*, 1989].

[55] In the present study, the extratropical tropopause appears as a very sharp interface on average. A number of studies on extratropical STE, however, suggest a picture of the extratropical tropopause as a layer of mixed tropospheric-

stratospheric properties: the "tropopause mixing layer" (see introduction). The present study shows the existence of a dynamically well mixed layer (the TIL) just above the tropopause which about coincides with the tropopause mixing layer [cp. *Hoor et al.*, 2005, Figure 1]. The strong stratification in the TIL on the one hand and large-scale horizontal mixing in the TIL on the other hand imply that air that is transported into the TIL from below tends to stay in the TIL but is mixed horizontally over large distances. It seems, then, that the tropopause mixing layer is not formed by frequent vertical mixing but rather by sporadic vertical mixing and subsequent horizontal redistribution. STE in this concept becomes the exception rather than the rule, underlining the importance of a detailed understanding of individual STE events.

[56] The sharpness of the tropopause has implications for the propagation of both Rossby and gravity waves. On the one hand the strong PV gradients associated with a sharp tropopause act as a Rossby wave guide [*Schwierz et al.*, 2004]. On the other hand upward propagation of waves through the tropopause is strongly inhibited by a sharp tropopause, mainly through the almost step-like behavior of N^2. In the case of Rossby waves the relevant parameter controlling the upward propagation is the so-called refractive index [*Charney and Drazin*, 1961], which maximizes at the tropopause. In the case of upward gravity wave propagation through the tropopause the respective refractive index is often called the Scorer parameter [e.g., *Gill*, 1982] which also maximizes at the tropopause. In both cases the large refractive index can lead to partial or even total wave reflection at the tropopause. The results of the present paper based on the TB average suggest a much stronger inhibition of upward wave propagation through the tropopause than that based on conventional averages. A detailed analysis of the impact of the observed thermal and wind structure around the extratropical tropopause (Figures 4 and 5) on upward wave propagation is a future task.

[57] The present study provides climatological evidence of an atmospheric layer (the above termed TIL) that lies above the extratropical tropopause and yet differs quite substantially from the stratosphere aloft in that it is much more strongly stably stratified. Large-scale dynamical mixing seems ubiquitous within the TIL, which further distinguishes this layer from the stratosphere aloft. These properties of the TIL suggest a distinct notation for it. We propose the term extratropical substratosphere (ESS) which emphasizes the location of this atmospheric layer: embedded within the stratosphere but with distinct properties. Noteworthily, the term "substratosphere" has been used already almost 100 years ago, shortly after the discovery of the tropopause, by *Shaw* [1912] and *Schmauß* [1913]. Recently it has been resuscitated by *Thuburn and Craig* [2002] in a slightly different context. A more detailed description of the dynamical, but also the chemical, radiative, and microphysical properties of the ESS is an obvious task for the future. It is also noted here that at present there seems to be a substantial lack of understanding of the processes that shape the ESS. On the dynamics side, emphasis has been on large-scale dynamical processes in the present study. However, even small-scale turbulence might be important within the ESS [*Joseph et al.*, 2003]. An understanding of the processes that shape the ESS is further complicated by the fact that the processes shaping the tropopause itself are not fully understood.

Appendix A: Determination of Tropopause

[58] As mentioned in section 3, only thermal tropopauses can be obtained from the radiosonde data. The WMO definition [*WMO*, 1957] is used to determine the thermal tropopause. This tropopause definition relies on the threshold γ_{TP} in the vertical temperature gradient γ. The much higher vertical resolution of the present data as compared to the data used half a century ago, however, calls for some care when applying the thermal tropopause criteria. As a test, the analysis in this paper has been repeated for one midlatitude station with slightly modified values of γ_{TP} (3 K km^{-1} and 1 K km^{-1}, respectively) with no obvious change in the results.

[59] First, the vertical temperature gradient is computed by means of centered differences for all altitudes z_i within a given profile: $\Delta_z T_i = (T_{i+1} - T_{i-1})/(z_{i+1} - z_{i-1})$. Then the smallest altitude (z_k) is obtained for which $\Delta_z T_k \geq \gamma_{TP}$. For $z \geq z_k$ the smallest altitude (z_j) is obtained for which $\langle \Delta_z T_{j,j+1,j+2} \rangle \geq \gamma_{TP}$ and $\langle \Delta_z T_{j-3,j-2,j-1} \rangle < \gamma_{TP}$ ($\langle . \rangle$ denotes the arithmetic average of all temperature gradients indicated by the subscripts). If $\langle \Delta_z T_{j,j+1,j+2} \rangle > 0$ then the tropopause altitude z_{TP} is assigned to the level of minimum temperature within the altitude range $[z_{j-3}, z_{j+2}]$ and the tropopause temperature T_{TP} is assigned to this minimum temperature. If, on the other hand, $\langle \Delta_z T_{j,j+1,j+2} \rangle \leq 0$ then z_{TP} is assigned to the level of intersection of two linear fits of $T(z)$ within the altitude ranges $[z_{j-3}, z_{j-1}]$ and $[z_j, z_{j+2}]$, respectively, and T_{TP} is assigned to the value of T at the level of intersection. Finally, the thus obtained z_{TP} is only accepted if $|z_{TP} - z_j| \leq 250$ m, $p_j < 500$ hPa (p is pressure), and if there exists no T_i within the altitude range $[z_{TP}, z_{TP} + 2$ km] for which $(T_i - T_{TP})/(z_i - z_{TP}) \leq \gamma_{TP}$ and $(T_{i+1} - T_{TP})/(z_{i+1} - z_{TP}) \leq \gamma_{TP}$.

[60] **Acknowledgments.** The free availability of the U.S. high-resolution radiosonde data through the SPARC data center at Stony Brook University, NY, USA, is highly acknowledged. Thanks to Ling Wang and Marv Geller for their support in getting started with the data. The main part of this work has been carried out within the Ph.D. work of the author under the supervision of Andreas Dörnbrack and Ulrich Schumann at DLR. Their steady interest in this work and valuable discussions are highly acknowledged. Most of the paper has been written at University of Toronto where the support, discussions, and critical reading of the manuscript by Ted Shepherd have been very helpful. Thanks for useful discussions to Michel Bourqui, George Craig, Marv Geller, Peter Haynes, Michaela Hegglin, Klaus-Peter Hoinka, Peter Hoor, Laura Pan, Kirill Semeniuk, Mel Shapiro, Heini Wernli, Volkmar Wirth, and Günther Zängl. Finally, the constructive criticism by two anonymous reviewers is acknowledged.

References

Ambaum, M. (1997), Isentropic formation of the tropopause, *J. Atmos. Sci.*, *54*, 555–568.

Baldwin, M. P., and T. J. Dunkerton (1999), Propagation of the arctic oscillation from the stratosphere to the troposphere, *J. Geophys. Res.*, *104*, 30,937–30,946.

Bethan, S., G. Vaughan, and S. J. Reid (1996), A comparison of ozone and thermal tropopause heights and the impact of tropopause definition on quantifying the ozone content of the troposphere, *Q. J. R. Meteorol. Soc.*, *122*, 929–944.

Birner, T. (2003), Die extratropische Tropopausenregion, *Res. Rep. DLR-FB-2004-17*, Dtsch. Zent. fr Luft- und Raumfahrt, Cologne, Germany.

Birner, T., A. Dörnbrack, and U. Schumann (2002), How sharp is the tropopause at midlatitudes?, *Geophys. Res. Lett.*, *29*(14), 1700, doi:10.1029/2002GL015142.

Charlton, A. J., A. O'Neill, W. A. Lahoz, and A. C. Massacand (2004), Sensitivity of tropospheric forecasts to stratospheric initial conditions, *Q. J. R. Meteorol. Soc.*, *130*, 1771–1792.

Charney, J. G., and P. G. Drazin (1961), Propagation of planetary scale disturbances from the lower into the upper atmosphere, *J. Geophys. Res.*, *66*, 83–109.

Dessler, A. E., E. J. Hintsa, E. M. Weinstock, J. G. Anderson, and K. R. Chan (1995), Mechanisms controlling water vapor in the lower stratosphere: "A tale of two stratospheres," *J. Geophys. Res.*, *100*, 23,167–23,172.

Egger, J. (1995), Tropopause height in baroclinic channel flow, *J. Atmos. Sci.*, *52*, 2232–2241.

Ertel, H. (1942), Ein neuer hydrodynamischer Wirbelsatz, *Meteorol. Z.*, *59*, 277–281.

Gill, A. E. (1982), *Atmosphere-Ocean Dynamics*, 662 pp., Elsevier, New York.

Hakim, G. J. (2005), Vertical structure of midlatitude analysis and forecast errors, *Mon. Weather Rev.*, *133*, 567–578.

Haynes, P., and E. Shuckburgh (2000), Effective diffusivity as a diagnostic of atmospheric transport: 2. Troposphere and lower stratosphere, *J. Geophys. Res.*, *105*, 22,795–22,810.

Haynes, P., J. Scinocca, and M. Greenslade (2001), Formation and maintenance of the extratropical tropopause by baroclinic eddies, *Geophys. Res. Lett.*, *28*, 4179–4182.

Hoerling, M. P., T. K. Schaak, and A. J. Lenzen (1991), Global objective tropopause analysis, *Mon. Weather Rev.*, *119*, 1816–1831.

Hoinka, K. P. (1998), Statistics of the global tropopause, *Mon. Weather Rev.*, *126*, 3303–3325.

Hoor, P., C. Gurk, D. Brunner, M. I. Hegglin, H. Wernli, and H. Fischer (2004), Seasonality and extent of extratropical TST derived from in-situ CO measurements during SPURT, *Atmos. Chem. Phys.*, *4*, 1427–1442.

Hoor, P., H. Fischer, and J. Lelieveld (2005), Tropical and extratropical tropospheric air in the lowermost stratosphere over Europe: A CO-based budget, *Geophys. Res. Lett.*, *32*, L07802, doi:10.1029/2004GL022018.

Hoskins, B. J. (1991), Towards a PV-θ view of the general circulation, *Tellus, Ser. AB*, *43*, 27–35.

Hoskins, B. J., M. E. McIntyre, and A. W. Robertson (1985), On the use and significance of isentropic potential vorticity maps, *Q. J. R. Meteorol. Soc.*, *111*, 877–946.

Joseph, B., A. Mahalov, B. Nicolaenko, and K. L. Tse (2003), High resolution DNS of jet stream generated tropopausal turbulence, *Geophys. Res. Lett.*, *30*(10), 1525, doi:10.1029/2003GL017252.

Lindzen, R. S., and M. Fox-Rabinovitz (1989), Consistent vertical and horizontal resolution, *J. Atmos. Sci.*, *46*, 2575–2583.

Manabe, S., and R. T. Wetherald (1967), Thermal equilibrium of the atmosphere with a given distribution of relative humidity, *J. Atmos. Sci.*, *24*, 241–259.

Müller, R., and G. Günther (2003), A generalised form of Lait's modified potential vorticity, *J. Atmos. Sci.*, *60*, 2229–2237.

National Climate Data Center (1998), Data documentation for data set rawinsonde 6-second data, *Tech. Rep. D6211*, Natl. Clim. Data Cent., Asheville, N. C.

NOAA/NASA/U.S. Air Force (1976), U.S. Standard Atmosphere 1976, technical report, U.S. Govt. Print. Off., Washington, D. C.

Pan, L., W. J. Randel, B. L. Gary, M. J. Mahoney, and E. J. Hintsa (2004), Definitions and sharpness of the extratropical tropopause: A trace gas perspective, *J. Geophys. Res.*, *109*, D23103, doi:10.1029/2004JD004982.

Peixoto, J. P., and A. H. Oort (1992), *Physics of Climate*, 520 pp., Springer, New York.

Reed, R. J. (1955), A study of a characteristic type of upper-level frontogenesis, *J. Meteorol.*, *12*, 226–237.

Santer, B. D., et al. (2003), Behavior of tropopause height and atmospheric temperature in models, reanalyses, and observations: Decadal changes, *J. Geophys. Res.*, *108*(D1), 4002, doi:10.1029/2002JD002258.

Schmauß, A. (1913), Die Substratosphäre, *Beitr. Phys. Atmos.*, *6*, 153–164.

Schneider, T. (2004), The tropopause and the thermal stratification in the extratropics of a dry atmosphere, *J. Atmos. Sci.*, *61*, 1317–1340.

Schwierz, C., S. Dirren, and H. C. Davies (2004), Forced waves on a zonally aligned jet stream, *J. Atmos. Sci.*, *61*, 73–87.

Shapiro, M. A. (1980), Turbulent mixing within tropopause folds as a mechanism for the exchange of chemical constituents between the stratosphere and the troposphere, *J. Atmos. Sci.*, *37*, 994–1004.

Shaw, N. (1912), Preface to "The free atmosphere in the region of the British Isles" by W. H. Dines, *Met. Off. London Geophys. Mem.*, *2*, 13–22.

Shepherd, T. G. (2002), Issues in stratosphere-troposphere coupling, *J. Meteorol. Soc. Jpn.*, *80*, 769–792.

Stohl, A., et al. (2003), Stratosphere-troposphere exchange: A review, and what we have learned from STACCATO, *J. Geophys. Res.*, *108*(D12), 8516, doi:10.1029/2002JD002490.

Thompson, D. W. J., and J. M. Wallace (1998), The arctic oscillation signature in the wintertime geopotential height and temperature fields, *Geophys. Res. Lett.*, *25*, 1297–1300.

Thorpe, A. J. (1986), Synoptic scale disturbances with circular symmetry, *Mon. Weather Rev.*, *114*, 1384–1389.

Thuburn, J., and G. C. Craig (2002), On the temperature structure of the tropical substratosphere, *J. Geophys. Res.*, *107*(D2), 4017, doi:10.1029/2001JD000448.

Untch, A., et al. (1999), Increased stratospheric resolution in the ECMWF forecasting system, *ECMWF Newsl.*, *82*, 2–8.

Wang, L., M. A. Geller, and M. J. Alexander (2005), Spatial and temporal variations of gravity wave parameters, part I: Intrinsic frequency, wavelength, and vertical propagation direction, *J. Atmos. Sci.*, *62*, 125–142.

Wirth, V. (2000), Thermal versus dynamical tropopause in upper-tropospheric balanced flow anomalies, *Q. J. R. Meteorol. Soc.*, *126*, 299–317.

Wirth, V. (2003), Static stability in the extratropical tropopause region, *J. Atmos. Sci.*, *60*, 1395–1409.

Wirth, V. (2004), A dynamical mechanism for tropopause sharpening, *Meteorol. Z.*, *13*, 477–484.

Wittman, M. A. H., L. M. Polvani, R. K. Scott, and A. J. Charlton (2004), Stratospheric influence on baroclinic lifecycles and its connection to the arctic oscillation, *Geophys. Res. Lett.*, *31*, L16113, doi:10.1029/2004GL020503.

World Meteorological Organization (1957), Meteorology—A three-dimensional science, *WMO Bull*, *6*, 134–138.

World Meteorological Organization (1986), Atmospheric ozone, *WMO Rep.*, *16*.

Zängl, G., and V. Wirth (2002), Synoptic-scale variability of the polar and subpolar tropopause: Data analysis and idealized PV inversions, *Q. J. R. Meteorol. Soc.*, *128*, 2301–2315.

T. Birner, Department of Physics, University of Toronto, 60 St. George Street, Toronto, ON, Canada, M5S 1A7. (thomas@atmosp.physics.utoronto.ca)